Metastable States of Dimethylammonium, $(CH_3)_2NH_2^{\bullet}$

Viet Q. Nguyen, Martin Sadilek, Jordan Ferrier, Aaron J. Frank, and František Tureček*

Department of Chemistry, Bagley Hall, Box 351700, University of Washington, Seattle, Washington 98195-1700

Received: December 16, 1996; In Final Form: March 19, 1997[⊗]

Hypervalent dimethylammonium radical, $(CH_3)_2NH_2^{\bullet}$, and its deuterium-labeled isotopomers $(CH_3)_2ND_2^{\bullet}$, $(CH_3)_2NHD^{\bullet}$, $(CD_3)_2NH_2^{\bullet}$, and $(CD_3)_2ND_2^{\bullet}$ were generated as transient species by collisional neutralization of their cations in the gas phase and studied by neutralization−reionization mass spectrometry, laser photoexcitation, and ab initio theory. $(CH_3)_2ND_2^{\bullet}$, $(CH_3)_2NHD^{\bullet}$, and $(CD_3)_2NH_2^{\bullet}$ gave fractions of metastable species of ≥ 3.3 μs lifetimes, whereas $(CH_3)_2NH_2^{\bullet}$ and $(CD_3)_2ND_2^{\bullet}$ dissociated completely on the same time scale. Metastable $(CD_3)_2NH_2^{\bullet}$ and $(CH_3)_2ND_2^{\bullet}$ were photoexcited but not photoionized with the combined 488 and 514.5 nm lines from an Ar-ion laser. Ab initio calculations with effective PMP4(SDTQ)/6-311++G-(3df,2p) identified the $(\tilde{X})^2A_1$ ground state of vertical ionization energy, $IE_v = 3.70$ eV. RRKM calculations on the ab initio potential energy surface of the $(\tilde{X})^2A_1$ state predicted predominant N−H and N−D bond dissociations but did not allow for competitive loss of CH_3 or CD_3. The four lowest excited states of $(CH_3)_2$-$NH_2^{\bullet}$, $(\tilde{A})^2B_1$, $(\tilde{B})^2A_1$, $(\tilde{C})^2B_2$, and $(\tilde{D})^2A_1$, were characterized by CIS/6-311++G(3df,2p) calculations, and their vertical ionization energies were calculated as 2.86, 2.57, 2.48, and 1.82 eV, respectively. The excited states were calculated to be strongly bound with respect to N−H bond dissociations. The N−C bond dissociations were interpreted by potential energy surface crossing of the $\tilde{B}$ and $\tilde{A}$ states and transitions via conical intersection to the dissociative ground state.

Introduction

Following Herzberg's discovery of $NH_4^{\bullet}$ in discharge in gaseous ammonia,[1−3] the chemistry of hypervalent ammonium,[4] oxonium,[5] and sulfonium[4d,6] radicals has been of much interest. Hypervalent onium radicals have formally nine electrons at the central heteroatom, and their electronic structures thus violate the octet rule.[7] Organic ammonium radicals derived from aliphatic amines have been generated by collisional neutralization of fast beams of ammonium cations and analyzed by neutralization−reionization mass spectrometry (NRMS).[8] Isotopomers of several radicals, such as ammonium,[4a] methylammonium,[4b] trimethylammonium,[9] and pyrrolidinium,[10] showed metastability on the microsecond time scale. In contrast, organic ammonium radicals that contained larger alkyl and aryl substituents[11] or functional groups[12] were found to dissociate completely within a few microseconds. Unimolecular dissociations of organic ammonium radicals often showed unexpected branching ratios in dissociations of N−H and N−C bonds that were difficult to interpret or predict on the basis of the known or estimated dissociation energetics[9] or using conventional reactivity rules.[13]

The energetics of hypervalent ammonium radicals was also addressed by several ab initio calculations.[14] $NH_4^{\bullet}$ was found to be weakly bound in its $^2A_1$ ground electronic state due to a ~40 kJ mol^{-1} potential energy barrier to exothermic dissociation by loss of H$^{\bullet}$. This low stability of $NH_4^{\bullet}$, as opposed to that of NH_4^+, which requires 523 kJ mol^{-1} for N−H bond homolysis, can be attributed to perturbation of the bonding orbitals in the radical by the presence of the unpaired electron.[14f] The four lowest excited electronic states of $NH_4^{\bullet}$ were calculated to be bound, and the energy barriers to their dissociations were predicted to increase as the odd electron was placed in Rydberg orbitals of increasing principal (n) and angular (l) quantum numbers.[14f] The ground and excited states of ammonium have been studied recently by photodissociation and photoionization experiments.[15,16] Boldyrev and Simons used ab initio calculations to study the ground electronic states of methylated ammonium radicals from mono- through tetramethylammonium.[17] All these radicals were found to be thermodynamically metastable with respect to exothermic dissociations by N−H or N−CH_3 bond cleavages. The first three members of the series showed decreasing activation energies for N−H bond dissociations, e.g., from 28 kJ mol^{-1} for methylammonium[17] to −8 kJ mol^{-1} for trimethylammonium.[9] The potential energy barriers to N−CH_3 bond cleavages were calculated to be within 50−60 kJ mol^{-1} for mono-, di-, and trimethylammonium.[9,17] However, the calculated energetics of ground electronic states in methylated ammonium radicals did not account completely for the behavior of these species when formed by collisional electron transfer. In particular, the microsecond metastability of trimethylammonium was incompatible with the dissociative energy profile along the N−H coordinate in the ground electronic state.[9] Furthermore, both N−H and N−C bond cleavages were observed experimentally in methylammonium and trimethylammonium, whose branching ratios were difficult to explain by the calculated potential energy barriers. Formation of excited states has been suggested to qualitatively explain the experimental data.[9] A metastable excited state has been found recently by photoionization of the related dimethyldeuteroxonium radical.[6]

To complete the series of studies on methylated ammonium radicals and provide experimental data for comparison with ab initio theory, we address in the present work the metastability and dissociations of dimethylammonium, $(CH_3)_2NH_2^{\bullet}$, **1H**$^{\bullet}$, and its isotopomers $(CH_3)_2ND_2^{\bullet}$ (**1D**$^{\bullet}$), $(CH_3)_2NHD^{\bullet}$ (**1HD**$^{\bullet}$), $(CD_3)_2$-$NH_2^{\bullet}$ (**2H**$^{\bullet}$), and $(CD_3)_2ND_2^{\bullet}$ (**2D**$^{\bullet}$). The formation of hypervalent radicals by collisional electron transfer and their analysis by NRMS have some specific features that have been discussed in detail previously.[8] Briefly, in NRMS a beam of precursor ions of a kiloelectronvolt kinetic energy is allowed to undergo

[⊗] Abstract published in *Advance ACS Abstracts,* May 1, 1997.

S1089-5639(96)04077-7 CCC: $14.00

glancing collisions with thermal molecules or atoms that serve as electron donors under single collision conditions. Electron transfer from a molecular donor to an ammonium cation acceptor is highly endothermic; for example, neutralization of dimethylammonium cations ($\mathbf{1H}^+$) with dimethyl disulfide is ~5.3 eV endothermic from the difference in the corresponding vertical ionization energies.[17,18] A small part of the ion kinetic energy is converted to make up for the energy deficit.[8] The interaction time between the electron donor and acceptor is limited to within $\sim 5 \times 10^{-15}$ s due to the ion velocity (1.85×10^5 m s^{-1} for 8200 eV $\mathbf{1H}^+$) and the short interaction path of ≤10 Å. The electron transfer can therefore be viewed as a vertical process.[8] Electron capture by the cation is not subject to dipole selection rules. Hence, excited electronic states in the radical are accessible depending on the Franck−Condon factors that govern the transition probabilities between the initial vibrational state of the precursor cation and the vibrational state of the hypervalent radical in the particular electronic state. The effect of the electron donor on the electron transition probabilities in fast collisions has been addressed qualitatively but is not well understood at present.[19] The precursor ion internal energy is known to have an effect on the formation of hypervalent radicals; as a rule, neutralization of vibrationally hot cations produces larger fractions of metastable radicals.[5e−g,8]

In this study we show that dimethylammonium radicals exhibit an intriguing pattern of metastability that depends on the presence and position of deuterium and the internal energy of the precursor cation. We also probe the excited states in $\mathbf{2H}^\bullet$ by laser photoexcitation at 2.41 and 2.54 eV and compare the experimental data with configuration interaction singles (CIS) calculations.[20] The dissociation kinetics and branching ratios are analyzed by Rice−Ramsperger−Kassel−Marcus (RRKM) calculations[21] on ab initio potential energy surfaces of ground state $\mathbf{1H}^\bullet-\mathbf{2D}^\bullet$.

Experimental Section

Methods. Measurements were made on a tandem quadrupole acceleration deceleration mass spectrometer, as described previously.[22] Precursor cations were generated in a tight chemical ionization source of our design. The ionization conditions were as follows: electron current 1 mA, electron energy 100 eV, ion source temperature 200−220 °C, ion energy 78−80 eV. The pressure of the protonation or deuteronation reagent gas was adjusted to obtain $[M + H]^+/ [M^{\bullet+}]$ or $[M + D]^+/[M^{\bullet+}]$ ratios >20 in most instances. This allowed us to keep the contributions from ^{13}C and ^{15}N isotopomers of dimethylamine cation-radicals below 0.1% of the $[M + H,D]^+$ ion intensities. The cations were extracted from the ion source, transmitted through a radio-frequency-only quadrupole mass analyzer, and accelerated to 8200 eV kinetic energy. Stable cations of >25 μs lifetimes were neutralized by collisions with dimethyl disulfide that was admitted to the collision cell at pressures such as to achieve 70% transmittance of the ion beam. This corresponded mostly (85%) to single-collision conditions. The remaining ions were reflected by a cylindrical lens maintained at +250 V, and the neutral products were allowed to drift through an electrostatic lens system (conduit)[23] to a downbeam collision cell. In addition to removing the precursor ions, the reflector lens also created a 16.5 kV/cm electrostatic field gradient that the neutral intermediates passed through. The lifetimes of the neutrals to be reionized and detected were 3.2−3.4 μs for $\mathbf{1H}^\bullet$ through $\mathbf{2D}^\bullet$ in the conventional NR mass spectra. The neutral intermediates were reionized by collisions with dioxygen admitted to the downbeam cell at pressures such as to achieve 70% transmittance of the precursor ion beam. The

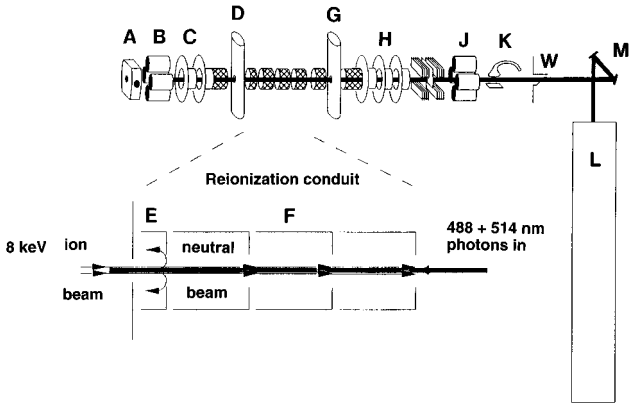

Figure 1. Schematic view of the tandem mass spectrometer for neutralization−photoexcitation−reionization. A, ion source; B,- quadrupole mass filter; C, acceleration lens; D, neutralization collision cell; E, reflector lens; F, conduit lens; G, reionization collision cell; H, deceleration lens; I, energy filter lens; J, quadrupole mass analyzer; K, electron multiplier; L, Ar-ion laser; M, mirrors; W, Brewster angle window.

NR conversions for $\mathbf{1H}^+$ through $\mathbf{2D}^+$, expressed as sums of integrated reionized peak intensities ($\sum I_{NR}$) relative to the intensity of the incident precursor ion beam (I_0), were $\sum I_{NR}/I_0 = (1.6 \pm 0.4) \times 10^{-5}$ from several measurements. The reionized cations were decelerated to 78 eV kinetic energy, energy filtered, and mass-analyzed by a quadrupole mass filter operated at unit mass resolution. The ion currents were detected by an electron multiplier, converted to voltages by a Keithley Model 428 amplifier, and treated by a PC-based data system.[22] Typically, 25−40 repetitive scans were accumulated per spectrum, and the spectra were reproduced in subsequent runs and over a period of several weeks. The apparatus was tuned daily to maximize the signal of reionized $CS_2^{\bullet+}$.

For laser photoexcitation experiments, the tandem mass spectrometer was equipped with an argon-ion laser, as described recently (Figure 1).[16,24] The neutralized beam passed through a 16.5 kV/cm electrostatic field gradient to remove high Rydberg states,[24,25] and it was merged with polarized light from a Laser Ionics 1400−12A Ar-ion laser operated in the power mode that delivered a total of 11 W at the 488 and 514.4 nm main visible lines. This corresponded to a 10^{19} photon/s flux of photons with 2.54 and 2.41 eV energy. The contributions from the 457, 476, 496, 501, and 528 nm lines were weaker than 0.9 W and extended the energy range from 2.36 to 2.72 eV. The laser beam overlapped with at least 40% of the neutral beam profile over the entire drift distance of 60 cm.[16,24] In the photoexcitation experiments, the electrostatic potentials on the conduit elements were scanned in link with the deceleration lens potentials to allow detection of survivor and product ions formed within the conduit between the deflector lens and the reionization cell (Figure 1, F).[16] This provided a 0.3−3.2 μs observation window for the neutral intermediates to be photoionized or collisionally reionized. This also increased the observation window for ion dissociations by 2.9 μs.[23]

The neutralization target is transparent at the wavelengths used. The UV spectrum of dimethyl disulfide ($\lambda_{max} = 258$ nm, $\epsilon_{max} = 21\,000$ in methanol) showed no absorption above 350 nm. The molar absorptivity at 488 and 514.5 nm was negligible ($\epsilon \ll 1$).

The laser beam entering the deceleration lens and the drift region was slightly collimated by the ion injection lens mounted on the quadrupole mass analyzer, whose internal diameter matched the laser beam width. This resulted in desorption/ionization of the adsorbed organics (mostly diffusion pump oil) that gave rise to the peaks of $C_3H_3^+$ at *m/z* 39 and $C_3H_5^+$ at

TABLE 1: Ab Initio Energies[a]

species		PMP2/6-31++G(d,p)	PMP4(SDTQ)/6-31++G(d,p)	PMP2/6-311++G(3df,2p)	PMP4[b]/6-311++G(3df,2p)
1H$^+$	$^1A_1$	−135.103 31[c]	−135.158 37[c]	−135.226 33	−135.281 39
1H$^+$	(VI)[d]			−135.225 23	
1H$^\bullet$	$(\tilde{X})^2A_1$	−135.232 94	−135.288 71	−135.359 30	−135.415 07
1H$^\bullet$	(VN)[e]	−135.231 76	−135.287 71	−135.358 15	−135.414 10
	$(\tilde{A})^2B_1$	−135.192 89	−135.248 74	−135.318 97	−135.375 82
	$(\tilde{C})^2B_2$	−135.181 43	−135.237 67	−135.305 76	−135.362 00

[a] In units of hartree, 1 hartree = 2625.5 kJ mol^{-1}. [b] From additivity approximation, eq 1. [c] From ref 17. [d] From vertical ionization of **1H**$^\bullet$. [e] From vertical neutralization of **1H**$^+$.

m/z 41, which did not interfere with the analyte peaks.[16] The *m/z* 39 and 41 peaks were observed in the absence of collision gases and precursor ions and were removed from the spectra by background subtraction. Over 100 repetitive scans were accumulated with the laser on and off in order to correct for reionization by background gas collisions. Raw data were digitally subtracted to obtain net differences due to photoionization or photodissociation. The differential ion currents were not measured directly; we estimate from these and previous measurements[16,24] that >0.1% changes in the reionized intensities were detectable.

Materials. Methane (Matheson, 99.97%), ammonia (Matheson, 99.99%), isobutane (Matheson, 99.5%), ND_3 (Cambridge Isotope Laboratories, 99% D), D_3O (Cambridge Isotope Laboratories, 99.5% D), isobutane-d_{10} (CND Isotopes, 99% D), and dimethylamine (Matheson, 99.5%) were used as received. $(CD_3)_2NH$ (**2**) was prepared by methylation of *p*-toluenesulfonamide with CD_3I (Cambridge Isotope Laboratories, 99.5% D) in ethanolic NaOH. The *N*,*N*-di-(methyl-d_6)-*p*-toluenesulfonamide, obtained in 67% yield, was hydrolyzed in refluxing 80% H_2SO_4 for 6 h; the $(CD_3)_2NH$ formed was liberated with NaOH and purified by trap-to-trap vacuum distillation. Yield, 65%, 99% D.

Calculations. Standard ab initio calculations were carried out using the Gaussian 92 suite of programs (Table 1).[26] The UHF/6-31++G(d,p) optimized geometries of **1H**$^\bullet$ and the transition states for loss of H$^\bullet$ and $CH_3^\bullet$ were obtained from previous calculations of Boldyrev and Simons[17] and used for vibrational analysis of **1H**$^\bullet$ and its isotopomers **1D**$^\bullet$, **1HD**$^\bullet$, **2H**$^\bullet$, and **2D**$^\bullet$. The harmonic vibrational frequencies and optimized geometries are available from the corresponding author upon request. The spin-projected energies[27] for **1H**$^+$, **1H**$^\bullet$, and the transition states were taken from the previous PMP4/6-31++G(d,p) + ZPVE data[17] unless stated otherwise. The geometries of **1H**$^+$ and **1H**$^\bullet$ were reoptimized with UMP2/6-31++G(2d,p). Single-point energies for **1H**$^+$ and the $(\tilde{X})^2A_1$ ground state of **1H**$^\bullet$ were obtained from PMP2(frozen core)/6-311++G(3df,2p) calculations on the reoptimized geometries. Effective PMP4(SDTQ)/6-311++G(3df,2p) energies were estimated from the additivity approximation[28] (eq 1).

$$\text{PMP4/6-311++G(3df,2p)} \approx \text{PMP4(SDTQ)/6-31++G(d,p)} + \text{PMP2/6-311++G(3df,2p)} - \text{PMP2/6-31++G(d,p)} \quad (1)$$

Geometry optimizations and potential-energy mapping along the N−H and N−C dissociation coordinates for the three lowest excited states of $(CH_3)_2NH_2^\bullet$ were carried out with the configuration interaction singles (CIS) method[20] using the 6-31++G(d,p) basis set. Single-point energies were obtained for the stationary states with CIS/6-311++G(3df,2p). RRKM calculations were carried out using Hase's program[29] on a cluster of Silicon Graphics Indigo workstations. Vibrational state densities were obtained by direct count for internal energies up to 60 kJ mol^{-1} above the dissociation threshold. At higher excitations, the state densities were obtained from the Whitten−Rabinovitch approximation.[30] The rotational states were treated adiabatically in the RRKM calculations.[31] The microscopic rate constants, $k(E,J,K)$, were Boltzmann-averaged over the thermal distribution of rotational J and K states pertinent to the ion source temperature. To this end, a short program was written to treat the output files of the RRKM calculations.

Results and Discussion

Metastable Dimethylammonium Radicals by Collisional Neutralization. Dimethylammonium cation **1H**$^+$ was prepared by gas phase protonations with CH_5^+, H_3O^+, t-$C_4H_9^+$, and NH_4^+ and by self-chemical ionization with $(CH_3)_2NH^{\bullet+}$, **1**$^{\bullet+}$. The corresponding reaction exothermicities[32] are given in eqs 2−6.

$$(CH_3)_2NH + CH_5^+ \rightarrow \mathbf{1H}^+ + CH_4 \qquad -\Delta H_r = 386 \text{ kJ mol}^{-1} \quad (2)$$

$$+ H_3O^+ \rightarrow \mathbf{1H}^+ + H_2O \qquad -\Delta H_r = 240 \text{ kJ mol}^{-1} \quad (3)$$

$$+ t\text{-}C_4H_9^+ \rightarrow \mathbf{1H}^+ + C_4H_8 \qquad -\Delta H_r = 129 \text{ kJ mol}^{-1} \quad (4)$$

$$+ NH_4^+ \rightarrow \mathbf{1H}^+ + NH_3 \qquad -\Delta H_r = 77 \text{ kJ mol}^{-1} \quad (5)$$

$$+ (CH_3)_2NH^{\bullet+} \rightarrow \mathbf{1H}^+ + (CH_3)_2N^\bullet \qquad -\Delta H_r = 25 \text{ kJ mol}^{-1} \quad (6)$$

The protonations were carried out at reagent gas pressures of ∼0.1 Torr allowing high conversions such as to achieve ion abundance ratios [**1H**$^+$]/[**1**$^{\bullet+}$] > 20 in most instances and similar for the isotopomers. This precaution was important in order to minimize contamination of **1H**$^+$ with ^{13}C and ^{15}N isotope satellites of **1**$^{\bullet+}$ which amounted to 2.6% of the latter ion intensity. Working in the high-pressure regime resulted in some cooling of the vibrationally excited cations, which underwent on average 70−90 collisions with the reagent gas during their calculated residence time in the ion source (5.9−8.2 μs). The neutralization−reionization spectra of **1H**$^+$ from protonations with CH_5^+, t-$C_4H_9^+$, NH_4^+, and **1**$^{\bullet+}$ are shown in Figure 2. The spectra showed weak peaks at *m/z* 46 (0.5−0.9% of the sum of reionized peak intensities, $\sum I_{NR}$) that corresponded by mass to reionized **1H**$^+$. Two major dissociation channels were observed (Scheme 1), i.e., loss of H$^\bullet$ to give dimethylamine (**1**), which appeared as **1**$^{\bullet+}$ at *m/z* 45 following ionization, and loss of CH_3 to give methylamine (**3**), which appeared as **3**$^{\bullet+}$ at *m/z* 31. Other products in the spectra were formed by ion dissociations of reionized **1**$^{\bullet+}$ (*m/z* 38−44, 26−29, 12−15) and **3**$^{\bullet+}$ (*m/z* 26−

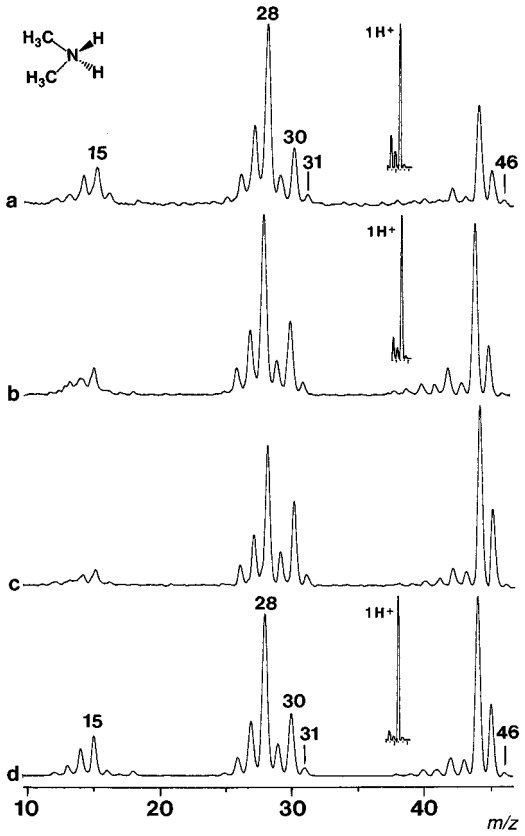

Figure 2. Neutralization (CH_3SSCH_3, 70% transmittance)−reionization (O_2, 70% transmittance) spectra of $\mathbf{1H}^+$ from protonation with (a) CH_5^+, (b) *t*-$C_4H_9^+$, (c) NH_4^+, (d) self-CI. Insets show the precursor ion relative intensities from chemical ionization.

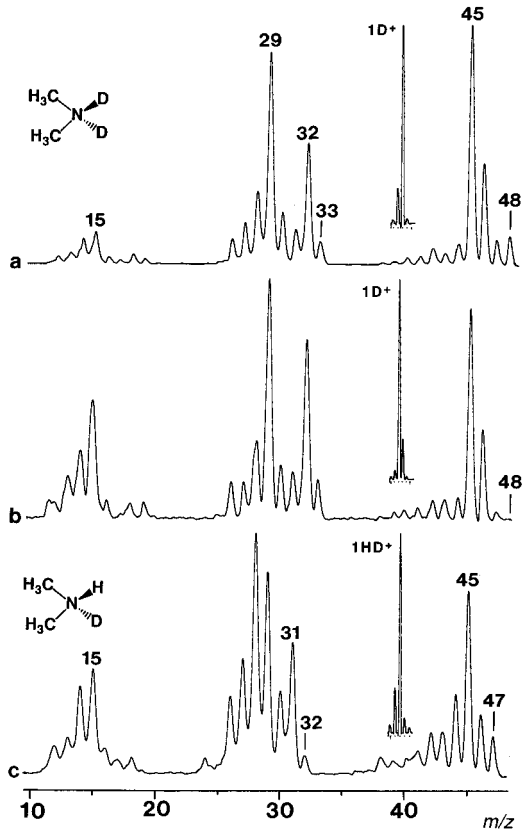

Figure 3. Neutralization−reionization spectra of $\mathbf{1D}^+$ from deuteronation with (a) ND_4^+, (b) D_3O^+, and (c) $\mathbf{1HD}^+$ from deuteronation with *t*-$C_4D_9^+$. Insets show the precursor ion relative intensities from chemical ionization.

SCHEME 1

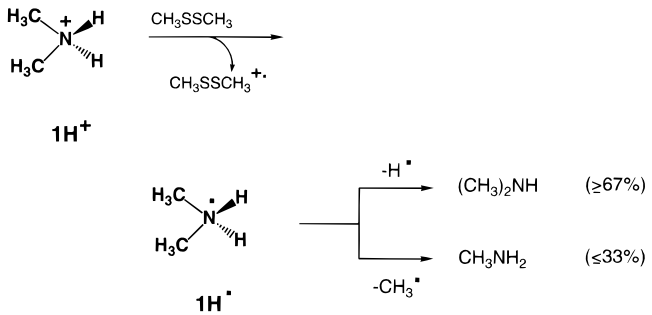

30, 12−16) as deduced from their reference NR spectra.[9,33] The peak at *m/z* 15 was notably stronger in the spectra of $\mathbf{1H}^+$ than in those of $\mathbf{1}^{\bullet+}$ and $\mathbf{3}^{\bullet+}$ and may correspond to reionized $CH_3^\bullet$ from dissociation of neutral $\mathbf{1H}^\bullet$.

The effect of precursor ion internal energy manifested itself in the relative abundances of secondary fragment ions, e.g., $HCN^{\bullet+}$ and $HCNH^+$, which were highest for the most energetic $\mathbf{1H}^+$ from protonation with CH_5^+. The $[\mathbf{3}^{\bullet+}]/[\mathbf{1}^{\bullet+}]$ ratio increased monotonously with the precursor ion internal energy from 0.13 for $\mathbf{1H}^+$ from self-CI to 0.27 for $\mathbf{1H}^+$ from protonation with CH_5^+. To obtain approximate branching ratios for the formation of neutral **1** and **3** from $\mathbf{1H}^\bullet$, the relative abundances of $\mathbf{1}^{\bullet+}$ and $\mathbf{3}^{\bullet+}$ in the NR spectrum of $\mathbf{1H}^+$ must be scaled by their fractions in the NR spectra of the neutral molecules, **1** and **3**, respectively, and by the reionization yields. These were estimated from the survivor to precursor ion intensity ratios for $\mathbf{1}^{\bullet+}$ (6×10^{-5}) and $\mathbf{3}^{\bullet+}$ (3.3×10^{-5}) in their NR spectra, giving a factor of 1.8 favoring $\mathbf{1}^{\bullet+}$. The corrected branching ratios indicated a 19/81 ratio for loss of $CH_3^\bullet$ and $H^\bullet$ from low-energy $\mathbf{1H}^\bullet$, which increased to 33/67 for dissociations of high-energy $\mathbf{1H}^\bullet$. Hence, loss of methyl was an important dissociation channel of $\mathbf{1H}^\bullet$.

The presence of surviving $\mathbf{1H}^+$ in the spectra was examined with regard to the possible contamination by $\mathbf{1}^{\bullet+}$ isotope satellites. For example, NR of $\mathbf{1H}^+$ from self-CI gave an 8×10^{-8} ratio of survivor to incident ion intensities, whereas the same ratio for $\mathbf{1}^{\bullet+}$ was measured as 6×10^{-5}. Hence, even the presence of a small fraction of ^{13}C and ^{15}N isotopomers of $\mathbf{1}^{\bullet+}$ coinciding by mass with $\mathbf{1H}^+$ (0.07% from the chemical ionization spectrum) contributed a large fraction (4×10^{-8}, 50%) to the survivor ion intensity. Likewise, isotope contamination was calculated to amount to 50, 200, and 110% of the survivor ion intensities in the NR spectra of $\mathbf{1H}^+$ from protonations with NH_4^+, *t*-$C_4H_9^+$, and CH_5^+, respectively. Considering the spread in the correction factors, it appeared safe to conclude that no significant fractions of survivor $\mathbf{1H}^\bullet$ were detected in collisional neutralizations of $\mathbf{1H}^+$.

Ions $\mathbf{1D}^+$ and $\mathbf{1HD}^+$ were generated by deuteronations at different exothermicities. $\mathbf{1D}^+$ was prepared by deuteronation with ND_4^+ and D_3O^+ of dimethylamine-*N*-*d*, whereas $\mathbf{1HD}^+$ was prepared by deuteronation of **1** with *t*-$C_4D_9^+$. The NR spectra of $\mathbf{1D}^+$ and $\mathbf{1HD}^+$ produced substantial fractions of survivor ions (Figure 3a,c). In this case, isotope corrections amounted to only 8 and 16% of the reionized $\mathbf{1D}^+$ and $\mathbf{1HD}^+$ intensities, respectively.[34] In contrast, $\mathbf{1D}^+$ from the more exothermic deuteronation with D_3O^+ gave a barely detectable survivor ion in the NR spectrum (Figure 3b). The existence of metastable $\mathbf{1D}^\bullet$ in the latter case was indirectly indicated by the peak at *m/z* 47, which was due to $H^\bullet$ loss from reionized $\mathbf{1D}^+$. Note that radical $\mathbf{1D}^\bullet$ can be expected to eliminate $D^\bullet$ but not $H^\bullet$. In contrast, dissociations of $\mathbf{1D}^+$ involved loss of both $H^\bullet$ and $D^\bullet$, as verified by its collision-induced dissociation spectrum. The observation of $H^\bullet$ loss in the NR spectrum of

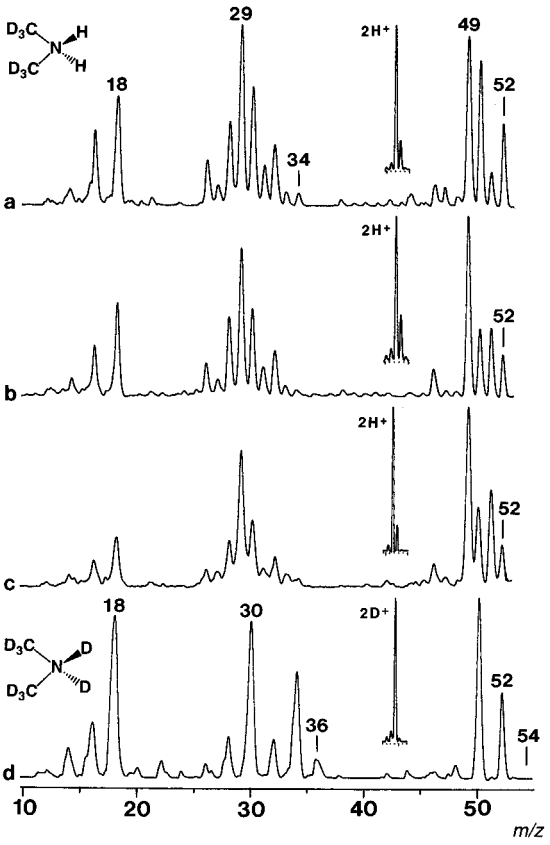

Figure 4. Neutralization−reionization spectra of $\mathbf{2H}^+$ from protonation with (a) CH_5^+, (b) *t*-$C_4H_9^+$, (c) self-CI, and (d) $\mathbf{2D}^+$ from deuteronation with ND_4^+. Insets show the precursor ion relative intensities from chemical ionization.

$\mathbf{1D}^+$ indicated unambiguously that a fraction of $\mathbf{1D}^\bullet$ survived for 3.3 μs and was reionized to $\mathbf{1D}^+$. Hence, the spectral data supported the existence of metastable $\mathbf{1D}^\bullet$ and $\mathbf{1HD}^\bullet$ but also pointed to substantial effects of the precursor ion internal energy. The corrected branching ratio for $CH_3^\bullet$ versus $D^\bullet$ loss from $\mathbf{1D}^\bullet$ (30/70) was higher than that for $CH_3^\bullet$ versus $H^\bullet$ loss from $\mathbf{1H}^\bullet$ (22/78) prepared from NH_4^+-protonated **1**. The branching ratio for the $CH_3^\bullet$ and $H^\bullet$ loss from $\mathbf{1HD}^\bullet$ (34/66) was similar to that for $\mathbf{1H}^\bullet$ (33/67) prepared from *t*-$C_4H_9^+$-protonated $\mathbf{1H}^+$. The NR spectrum of $\mathbf{1HD}^+$ also allowed us to evaluate the fractions of $(\mathbf{1HD} - H)^{\bullet+}$ and $(\mathbf{1HD} - D)^{\bullet+}$ after correcting for the consecutive loss of $H^\bullet$ from the former ion. The corrected ratio, $[\mathbf{1HD} - H]^{\bullet+}/[\mathbf{1HD} - D]^{\bullet+} = 1.64$, indicated a modest intramolecular isotope effect[35] favoring cleavage of the N−H bond in $\mathbf{1HD}^\bullet$.

Substantial fractions of survivor ions were obtained from neutralization−reionization of $\mathbf{2H}^+$ prepared by protonations of $(CD_3)_2NH$ (**2**) with CH_5^+ and *t*-$C_4H_9^+$ and by self-CI (Figure 4a−c). Isotope corrections to the intensity of survivor $\mathbf{2H}^+$ were <8% in each case. $\mathbf{2H}^+$ from CH_5^+-protonated **2** gave the largest fraction of metastable hypervalent dimethylammonium, $\mathbf{2H}^\bullet$, yielding 5% of reionized $\mathbf{2H}^+$ relative to $\sum I_{NR}$, and the highest branching ratio for loss of $CD_3^\bullet$ versus $H^\bullet$ (42/58). The other spectra (Figure 4b,c) showed lower fractions of survivor $\mathbf{2H}^+$ (3.0−3.4% $\sum I_{NR}$) and increased fractions of $\mathbf{2}^{\bullet+}$ which was formed by loss of $H^\bullet$ followed by reionization.

In contrast to $\mathbf{2H}^+$, no survivor ions were found for the fully deuterated isotopomer $\mathbf{2D}^+$ prepared by deuteronation of **2** with ND_4^+ (Figure 4d). The intermediate hypervalent radical $\mathbf{2D}^\bullet$ dissociated completely by $CD_3^\bullet$ and $D^\bullet$ losses in a 32/68 ratio. This result was qualitatively similar to the previous observation for the $C_2H_7O^\bullet$ system, where $CD_3CD_2OD_2^\bullet$ showed no metastability whereas other isotopomers did.[5g]

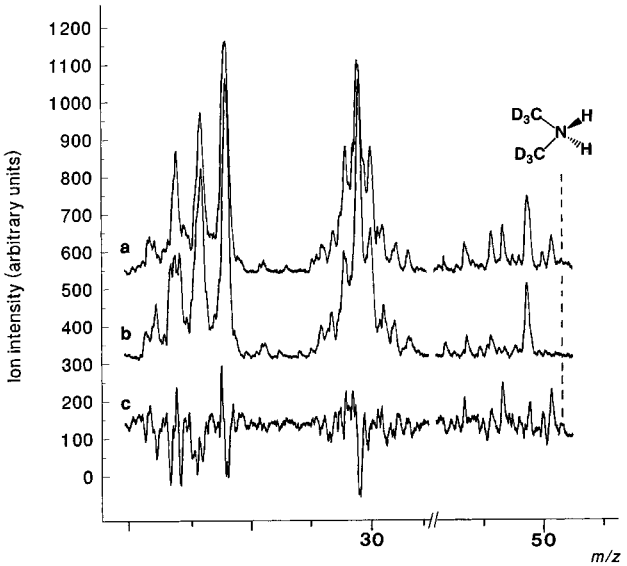

Figure 5. Neutralization−photoionization spectrum of $\mathbf{2H}^+$: (a) total spectrum with laser on; (b) collisional background with laser off; (c) background-corrected photoionization spectrum.

Laser Photoexcitation. We have further probed metastable radicals $\mathbf{2H}^\bullet$ and $\mathbf{1D}^\bullet$ by laser photoexcitation. In one series of experiments, metastable $\mathbf{2H}^\bullet$ from neutralization of CH_5^+-protonated **2** was exposed to the laser beam in the absence of the reionization gas. The resulting spectrum (Figure 5a) showed a small peak of $\mathbf{2H}^+$ at *m/z* 52 due to photoionization, while substantial peaks of fragment ions originating from $\mathbf{2H}^\bullet$ were observed. Subtraction of the collisional background (Figure 5b) and the laser background gave a spectrum (Figure 5c) that showed weak positive contributions from the dehydrogenation products of $\mathbf{2H}^\bullet$ at *m/z* 49−51 and negative contributions for $CDNH^+$ (*m/z* 29) and CD_3^+ (*m/z* 18). The net contribution to the peak of $\mathbf{2H}^+$ due to photoionization was within the noise level in the background-corrected spectrum (Figure 5c). Very similar results were obtained for photoionization of $\mathbf{1D}^\bullet$, whose background-corrected spectrum yielded a very small peak of $\mathbf{1D}^+$ due to laser photoionization. The data thus showed that photoionization of $\mathbf{1D}^\bullet$ and $\mathbf{2H}^\bullet$ was inefficient at the wavelengths used. This indicated that the vertical ionization energy of metastable dimethylammonium was greater than 2.41−2.54 eV from the Ar-ion main lines or that metastable $\mathbf{2H}^\bullet$ and $\mathbf{1D}^\bullet$ were photoionizable but the photoionization cross sections were too small to permit ion detection.

In a second series of experiments, the beams of metastable $\mathbf{1D}^\bullet$ and $\mathbf{2H}^\bullet$ were exposed to the laser beam in the presence of dioxygen which was admitted to the neutral drift region at a pressure allowing mostly (>85%) single-collision conditions. In this case, metastable $\mathbf{1D}^\bullet$ or $\mathbf{2H}^\bullet$ could undergo competitive unimolecular dissociations and photoexcitation, both followed by collisional reionization. Contributions from laser photoionization were excluded by the previous experiments. Following background corrections, the spectrum of $\mathbf{2H}^\bullet$ (Figure 6) showed positive contributions for reionized $\mathbf{2H}^+$ and its dissociation products due to irradiation. The increased intensity of $\mathbf{2H}^+$ must be due to interaction with photons of *neutral* $\mathbf{2H}^\bullet$, because alkylammonium ions and the neutralization and reionization gases are transparent at the wavelengths used.[36] The increased intensities of fragments may, in principle, be due to photodissociation of reionized $\mathbf{1}^{\bullet+}$ and $\mathbf{3}^{\bullet+}$, which were exposed to the laser beam for most of their path length through the mass spectrometer (Figure 1). **1** and **3** show large gaps (>2.5 eV) between the first and second bands in their photoelectron spectra,[37] which indicated that absorption of 2.41 and 2.54 eV

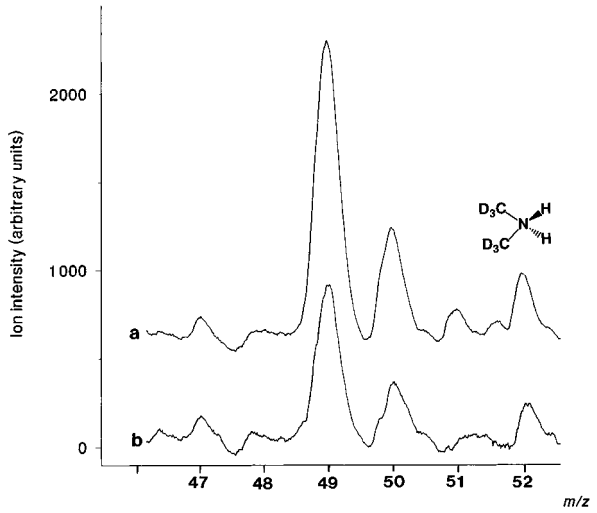

Figure 6. Neutralization−photoexcitation-reionization spectrum of $\mathbf{2H}^+$: (a) spectrum with laser on; (b) background-corrected spectrum.

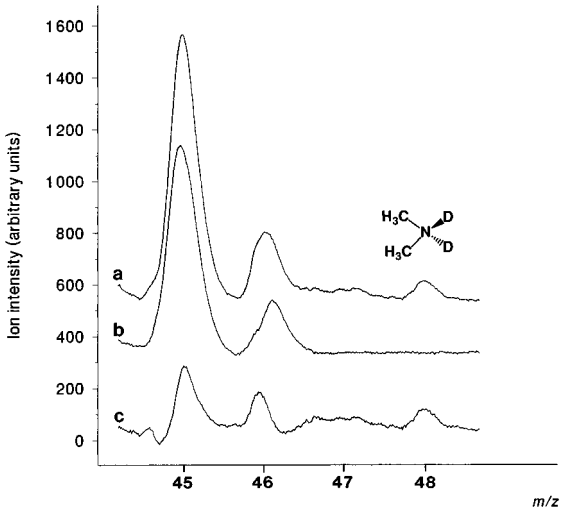

Figure 7. Neutralization−photoexcitation−reionization spectrum of $\mathbf{1D}^+$ from deuteronation with D_3O^+: (a) spectrum with laser on; (b) spectrum with laser off; (c) background-corrected spectrum.

photons could occur only in vibrationally hot $^2A'$ and ^2A ground electronic states of $\mathbf{1}^{\bullet+}$ and $\mathbf{3}^{\bullet+}$, respectively. The excited states of $\mathbf{1}^{\bullet+}$ and $\mathbf{3}^{\bullet+}$ are dissociative.[33] We found that methyl, dimethyl, and trimethylamine cation-radicals from neutralization and reionization showed only small increases of fragment relative intensities upon irradiation at 488 and 514.5 nm, which were difficult to quantify.[16]

A large increase of survivor ion relative intensity was observed for photoexcitation of $\mathbf{1D}^\bullet$ from neutralization of D_3O^+-deuteronated **1**. In the absence of the laser beam the spectrum showed no detectable survivor $\mathbf{1D}^+$ for neutral observation times of 3.3 μs (Figure 3b) or 0.3 μs (Figure 7b). However, irradiation of $\mathbf{1D}^\bullet$ in the neutral drift region resulted in the formation of a fraction of survivor $\mathbf{1D}^+$ (Figure 7a,c). Since $\mathbf{1D}^\bullet$ was not photoionized at the wavelengths used, the increased intensity of survivor $\mathbf{1D}^+$ must be due to photoexcitation of $\mathbf{1D}^\bullet$ followed by collisional reionization of the photoexcited state.

The processes involved in the previous photoexcitation experiments are summarized in Scheme 2. Metastable radicals P(0), formed by collisional neutralization in an initial electronic state (0), can undergo competitive collisional reionization to give survivor ions P^+ or unimolecular dissociation to products. Upon irradiation these two processes compete with photoexcitation followed by dissociation or collisional reionization of the excited state P(1). Direct photoionization of P(0) was excluded experimentally (vide supra). Photoionization of photoexcited states would correspond to a two-photon process that was deemed unlikely at the photon densities used. Under these assumptions, the formation of P^+ from P(0) was due entirely to collisional ionization as described by eq 7, which gave eq 8 on integration.

SCHEME 2

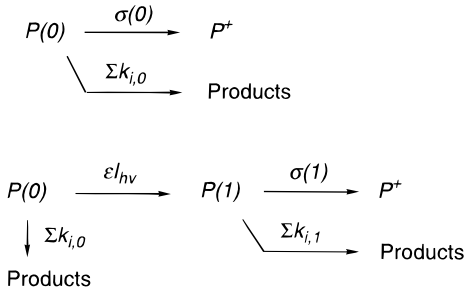

$$dP^+(0) = P(0)_{l=0} \exp(-\sum_i k_i l/v)\sigma(0)N\, dl \quad (7)$$

$$P^+(0) = P(0)_{l=0}\, \sigma(0)N(v/\sum_i k_i)[1 - \exp(-\sum_i k_i L/v)] \quad (8)$$

$P(0)_{l=0}$ is the initial flux of neutral $\mathbf{1H}^\bullet$ (or its isotopomers) in the electronic state produced by neutralization, $P^+(0)$ is the flux of reionized $\mathbf{1H}^+$, $\sigma(0)$ is the collisional ionization cross section, k_i are the unimolecular dissociation constants, N is the reionization gas number density, v is the neutral velocity, dl is the path length element for P(0), and L is the total neutral path length. The dissociation kinetics of P(0) was approximated by single exponential decay in this model. The effect of photoexcitation on the population of P(0) was neglected. Following photoexcitation, the excited state P(1) is collisionally ionized to form P^+ according to eqs 9−11, where ds is the path element for P(1) ($s + l = L$), ϵ is the photoexcitation cross section, $I_{h\nu}$

$$P(1)_l = P(0)_{l=0}\epsilon I_{h\nu}(v/\sum_i k_i)[1 - \exp(-\sum_i k_i l/v)] \quad (9)$$

$$dP^+(1) = P(1)_l\, \sigma(1)N\, ds \quad (10)$$

$$P^+(1) = P(0)_{l=0}\epsilon I_{h\nu}\sigma(1)N(v/\sum_i k_i)\{L - (v/\sum_i k_i)[1 - \exp(-\sum_i k_i L/v)]\} \quad (11)$$

is the light intensity, and $\sigma(1)$ is the collisional ionization cross section for P(1). Built in this model are the simplifying assumptions that the excited state is not depleted by dissociations and de-excitation. The flux of reionized P^+ depends on several parameters, in particular $\sum_i k_i$, which determine the half-life of P(0). For example, dissociations with rate constants $>3 \times 10^7$ s^{-1} would leave <0.5% of nondissociated $\mathbf{1H}^\bullet$ to be reionized on the present time scale. However, the *relative enhancement* of P^+ intensity upon irradiation, expressed as $P^+(1)/P^+(0)$, which is amenable to experimental measurements, showed some general characteristics that are now discussed.

Photoexcitation of $\mathbf{1H}^\bullet$, in the form of its metastable isotopomers $\mathbf{1D}^\bullet$ or $\mathbf{2H}^\bullet$, must involve promoting the odd electron from the diffuse, singly occupied, $7a_1$ molecular orbital to a higher orbital of a Rydberg type.[14,17] Considering for simplicity hydrogen-like ns orbitals ($n \geq 3$), the effective orbital radius, taken at the maximum of the radial distribution function,[38] scales roughly with the square of the principal quantum number, n^2, so that the collisional ionization cross section scales roughly

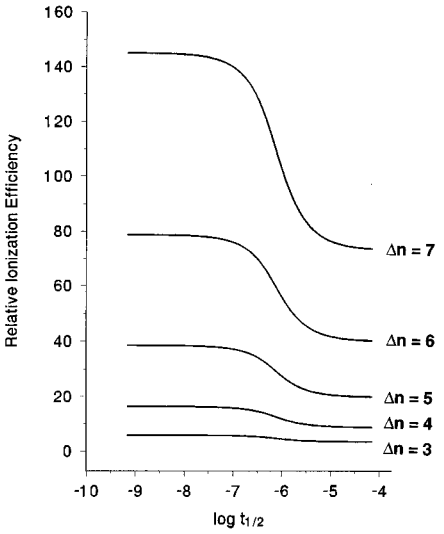

Figure 8. Relative enhancement of ionization yields for $ns \rightarrow (n + \Delta n)s$ excitations. $t_{1/2} = \ln 2/\sum k_i$ is the neutral half-life.

with n^4. Hence, a higher n state can be expected to have a substantially larger ionization probability than a lower n state. A very similar situation is encountered in multiphoton ionization, where the photoionization cross sections of excited states are several orders of magnitude greater than those of the corresponding ground states.[39] The relative enhancement, $P^+(1)/P^+(0)$, depends on the half-life of P(0) ($t_{1/2} = \ln 2/\sum_i k_i$) and the photoexcitation yield. This is plotted in Figure 8 for $n = 3$ and an arbitrary 1/10 ratio of photoexcitation and collisional reionization yields for P(0). The relative enhancement increases steeply for neutrals of half-lives in the $10^{-5}-10^{-7}$ s range, whereas the total fraction of surviving radicals decreases in the same order. This means that short-lived but observable **1D•** or **2H•** will give the greatest *relative* enhancement of survivor $\mathbf{1D}^+$ or $\mathbf{2H}^+$, respectively, upon photoexcitation. This was indeed observed for photoexcitation of metastable **1D•** and **2H•**, where the less abundant $\mathbf{1D}^+$ gave a greater enhancement than the more abundant $\mathbf{2H}^+$ (Figures 6 and 7). Figure 8 also shows that the enhanced reionization yield upon photoexcitation depends strongly on the change in n and can exceed 10^2 for excitations from $n = 3$ to $n = 10$. It is also pertinent to note that the lifetimes of high Rydberg states scale with n^3;[40] photoexcitation to high Rydberg states is therefore expected to increase the metastable lifetimes and hence the probability for collisional reionization.

Although the experimental data provided a qualitative description of metastable dimethylammonium radicals, alone they did not allow us to identify the electronic states responsible for the observed metastability. To summarize the experiments, the metastable state(s) were not photoionized with 2.41 and 2.54 eV photons, but underwent photoexcitation that caused a large change in the ionization cross section. These results are now examined in the light of ab initio and RRKM calculations.

Ground and Excited State Energetics. The energetics of the $^2A_1$ ground electronic state of **1H•** was studied previously by Boldyrev and Simons at the UMP4(SDTQ)/6-31++G(d,p) level of ab initio theory.[17] The radical was found to be weakly bound with respect to N−H bond cleavage, whereas an energy barrier was found for the cleavage of the N−CH_3 bond (Figure 9). Both dissociations were found to be exothermic; the calculated difference in the product enthalpies (72 kJ mol^{-1}, Figure 9) was close to the difference in the product heats of formation (77 kJ mol^{-1}).[18]

We used the previous ab initio energies and optimized structures to obtain zero-point corrections, harmonic frequencies,

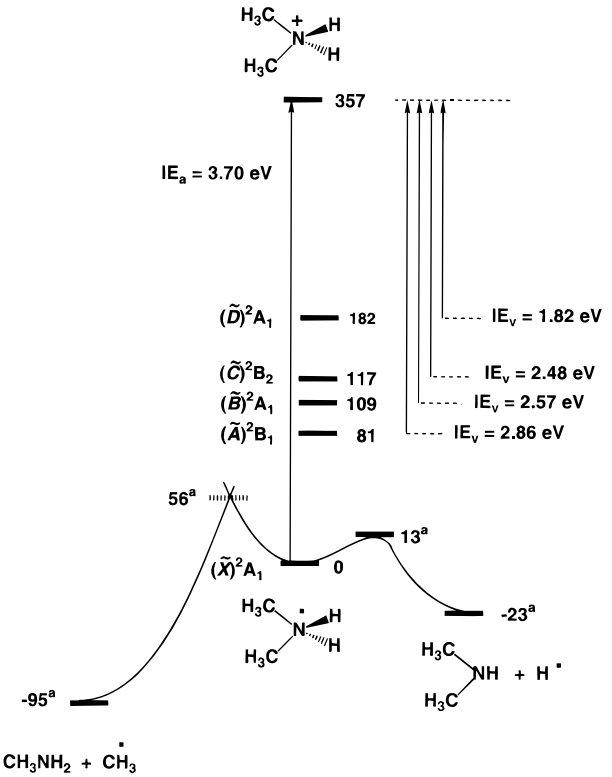

Figure 9. Energy diagram for excitation, ionization, and dissociation in **1H•**. The ground-state ionization energy is from PMP4/6-311++G(3df,2p) calculations. The excited-state ionization energies are from CIS/6-311++G(3df,2p) excitation energies and the ground-state ionization energy. [a]Ground-state energy data from ref 17.

and moments of inertia for the isotopomers and the relevant transition states that were used in RRKM calculations of unimolecular rate constants for dissociations of **1H•**, **1HD•**, **1D•**, **2H•**, and **2D•**. A complicating factor was the finding that the highest point on the potential energy surface along the N−CH_3 dissociation coordinate was not a saddle point but a cusp that was located at a bond length d(N−C) = 1.81 Å. An analogous discontinuity on the potential energy surface was obtained for the N−CH_3 bond dissociation in trimethylammonium.[9] Nevertheless, harmonic frequency analysis at the cusp gave a single negative force constant for the motion along the N−C coordinate, and so this point was used to approximate the transition state for the methyl loss. The RRKM curves for the dissociations of **1H•** (Figure 10a) showed that the loss of H• should be preferred at all excitations. The experimental branching ratio for CH_3• versus H• loss (0.23) could be achieved in dissociations of **1H•** at excitations >100 kJ mol^{-1} above the dissociation threshold, while much greater ratios were predicted by RRKM rate constants for lower excitations (Figure 10). A similar conclusion followed from the RRKM curves for **1D•**. In contrast, the experimental branching ratios for loss of CD_3 versus H• from **2H•** (0.72) and loss of CD_3• versus D• from **2D•** (Figure 10b) could not be explained by the RRKM curves at excitations <140 kJ mol^{-1} above the threshold. RRKM curves for the H• versus D• loss from **1HD•** predicted large intramolecular isotope effects, as shown in Figure 11. The calculated k_H/k_D ratio approached the experimental value (1.6) at excitation energies >140 kJ mol^{-1}.

In contrast, the metastability observed for **1HD•**, **1D•**, and **2H•** required that there be a fraction of radicals with internal energies below the activation barrier for the lowest energy dissociation by N−H or N−D bond cleavage. The calculated lowest activation energies for the $(\tilde{X})^2A_1$ state of **1H•**, **1HD•**, **1D•**, **2H•**, and **2D•**, including zero-point corrections, e.g., 13,

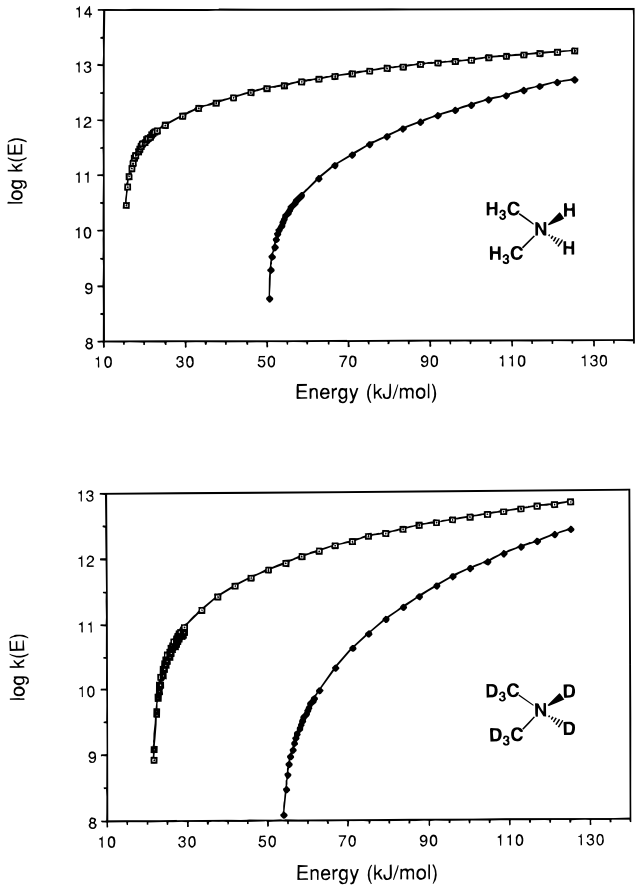

Figure 10. RRKM rate coefficients for unimolecular dissociations of **1H•** and **2D•** on the ground-state potential energy surface: open squares, N−(H,D) bond cleavage; full diamonds, N−C bond cleavage. The lower parts of the curves show superimposed points from direct count calculations.

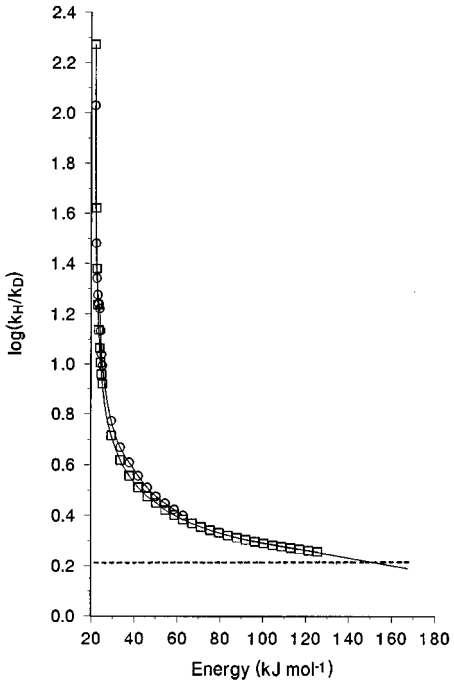

Figure 11. RRKM isotope effect on N−H and N−D bond dissociations in **1HD•**: open circles, direct count; open squares, Whitten−Rabinovitch approximation; dashed line, experimental value.

15, 21, 16, and 22 kJ mol^{-1}, respectively, were very low and did not suggest any particular stabilization of **1HD•** and **2H•** nor destabilization of **2D•**. Hence, barring the unlikely possibility of a sharply bimodal internal energy distribution in **1HD•**, **1D•**, and **2H•**, the ground state properties of the radicals could not account for the observed metastability, dissociations, and isotope effects.

The energetics of the electronic states in **1H•** were further investigated by ab initio calculations. The ground-state geometry was reoptimized with UMP2(FULL)/6-31++G(2d,p) calculations, which gave bond lengths and angles which were similar to those from previous UHF/6-31++G(d,p) calculations.[17] The optimized geometry was used for UMP2 single-point calculations using the larger 6-311++G(3df,2p) basis set. Population analysis of the HF/6-311++G(3df,2p) wave function of the ground state indicated the electron configuration in **1H•** to be $(a_1)^2(b_2)^2(a_1)^2(a_1)^2(b_2)^2(a_1)^2(b_1)^2(a_1)^2(b_2)^2(a_2)^2(a_1)^2(b_1)^2(b_2)^2$-$(a_1)^1...(a_1)^0(b_1)^0(b_2)^0(a_1)^0(b_1)^0$.... The energy of the $7a_1$ singly occupied orbital was 12.80 eV above the highest doubly occupied $4b_2$ orbital. This large separation made the system suitable for calculations by the CIS method, because all single-electron excitations involved exclusively the unpaired electron and combinations of the $7a_1$ SOMO and the virtual orbitals. Geometry optimizations with CIS/6-31++G(d,p) found the first three excited states of **1H•** as $(\tilde{A})^2B_1$, $(\tilde{B})^2A_1$, and $(\tilde{C})^2B_2$. The optimized geometry of the $\tilde{A}$ state was similar to that of the ground state; e.g., the respective N−H bond lengths were d(N−H) = 1.023 and 1.022 Å, while the respective N−C bond lengths were d(N−C) = 1.483 and 1.477 Å. The $\tilde{B}$ and $\tilde{C}$ states showed shorter N−H bonds (1.005 and 1.005 Å, respectively) and longer N−C bonds (1.499 and 1.498 Å, respectively). The CIS energies are summarized in Table 2. The relative energies for the equilibrium structures are given as the corresponding ionization energies in Figure 9.

The calculations indicated that neutralization of $\mathbf{1H}^+$ and ionization of the ground and three lowest excited electronic states of **1H•** were subject to negligible Franck−Condon effects ($\leq$3 kJ mol^{-1}). The adiabatic ionization energy of $(\tilde{X})^2A_1$ **1H•** was calculated by effective PMP4/6-311++G(3df,2p) as 3.70 eV, including zero-point energy corrections. In the absence of Franck−Condon effects, the vibrational energy distribution in the precursor ions must be largely preserved in the radicals formed by vertical neutralization.[33] The average vibrational energy in thermal $\mathbf{1H}^+$−$\mathbf{2D}^+$ ranged between 14.2 and 15.7 kJ mol^{-1} at 473 K. Thus, even fully thermalized precursor ions would produce dimethylammonium radicals with internal energies close to the dissociation barrier for the H or D loss from the ground electronic state. Efficient tunneling for the H loss could be expected.[25b] Moreover, neutralization of vibrationally excited ions from the exothermic protonations should give dimethylammonium radicals in dissociative vibrational states. Hence the formation of metastable $(\tilde{X})^2A_1$ states of microsecond lifetimes appeared highly improbable for the isotopomers of **1H•**. A chemical rationale for the weak N−H_N bonds in the $(\tilde{X})^2A_1$ electronic state of **1H•** can be inferred from the charge and spin densities, obtained from Mullikan population analysis of the UHF/6-311++G(3df,2p) wave function. The $(\tilde{X})^2A_1$ state showed a large spin population on the H_N atoms (+0.81). In addition, the negative charge on H_N (−0.54) and N (−0.57) and the antibonding character of the $7a_1$ SOMO along the N−H bond pointed to its facile dissociation.

The energies of the excited states were calculated by CIS/6-311++G(3df,2p) as 0.84, 1.13, 1.22, and 1.88 eV above the ground state for $(\tilde{A})^2B_1$, $(\tilde{B})^2A_1$, $(\tilde{C})^2B_2$, and $(\tilde{D})^2A_1$, respectively. The potential energy surfaces for the $\tilde{A}$, $\tilde{B}$, and $\tilde{C}$ states were investigated by CIS/6-31++G(d,p) calculations along the N−H and N−C coordinates; the bond lengths were changed stepwise, while the other degrees of freedom were fully

TABLE 2: CIS Energies and Oscillator Strengths

method		energy[a] oscillator strength, f[b] $\tilde{A}$	$\tilde{B}$	$\tilde{C}$	$\tilde{D}$
		Optimized Structures			
CIS/6-31++G(d,p)		−134.713 040	−134.702 460	−134.699 305	
CIS/6-311++G(3df,2p)		−134.749 517	−134.738 949	−134.735 799	−134.712 363[c]
		(0.226)	(0.102)	(0.201)	(0.048[c])
		Reaction Paths			
	d(N−H) (Å)				
CIS/6-31++G(d,p)	1.15	−134.701 459	−134.686 604	−134.683 371	
		(0.192)	(0.079)	(0.179)	
	1.25	−134.678 824	−134.661 537	−134.657 985	
		(0.123)	(0.064)	(0.139)	
	1.35	−134.649 484	−134.629 459	−134.625 563	
		(0.061)	(0.054)	(0.095)	
	d(N−C) (Å)				
CIS/6-31++G(d,p)	1.65	−134.701198	−134.695187	−134.690611	
		(0.246)	(0.093)	(0.178)	
	1.75	−134.687 366	−134.687 043	−134.679 132	
		(0.254)	(0.059)	(0.162)	
	1.85	−134.673 044	−134.685 876	−134.665 299	
		(0.243)	(0.002)	(0.145)	

[a] In units of hartree. [b] Oscillator strength given in parentheses. [c] On optimized geometry of the $\tilde{A}$ state.

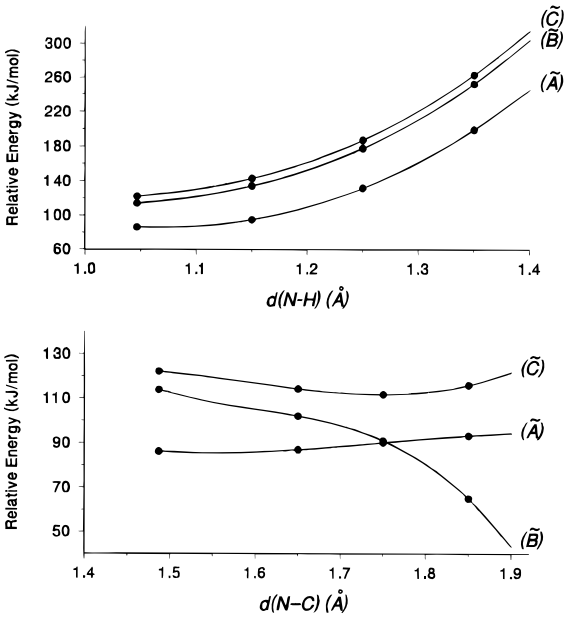

Figure 12. CIS/6-31++G(d,p) potential energy profiles along the N−H (top) and N−C (bottom) coordinates in **1H•**. The energies are relative to those of the ground state at the given bond distances.

optimized. The calculations showed that the $\tilde{A}$, $\tilde{B}$, and $\tilde{C}$ states were strongly bound with respect to N−H bond cleavage. Figure 12 shows that the excited state energies increased by >180 kJ mol^{-1} relative to the ground state as the N−H bond was stretched from the equilibrium length to 1.35 Å. The latter distance corresponded to the transition state of N−H bond dissociation on the ground-state potential energy surface.[17]

However, the excited state energies along the N−C coordinate differed (Figure 12, bottom). The $\tilde{A}$ and $\tilde{C}$ state energies roughly followed the ground state energy profile, indicating potential energy barriers to N−C bond dissociations in these excited states. Both states also showed substantial positive energy gradients at d(N−C) = 1.85 Å, indicating further potential energy increase at larger separations. In contrast, the $\tilde{B}$ state showed a small energy gradient upon stretching the N−C bond, and its energy converged to that of the ground state. This convergence also resulted in the $\tilde{A}$ and $\tilde{B}$ state potential energy surfaces crossing at d(N−C) ≈ 1.75 Å. The energy convergence and state symmetries ($^2A_1 \rightarrow A'$ for both $\tilde{X}$ and $\tilde{B}$) indicated that the $\tilde{X}$ and $\tilde{B}$ states nonadiabatically mix in the vicinity of the transition state for the N−C bond cleavage in **1H•**, possibly through a conical intersection.[41] The interaction between the $\tilde{X}$ and $\tilde{B}$ states gives a clue to the observed loss of methyl from **1H•**. The $(\tilde{B})^2A_1$ state of **1H•** can lose a methyl through internal conversion to the ground state at d(N−C) ≈ 1.85 Å. Since the potential energy surface of the ground state has a negative gradient at d(N−C) > 1.85 Å (Figure 9), the system cannot recross the transition state and continues moving along the N−C coordinate to break the bond and form $CH_3^\bullet$ and H_2NCH_3. The overall dissociation, $(\tilde{B})^2A_1 \rightarrow CH_3^\bullet + H_2NCH_3$, is >200 kJ mol^{-1} exothermic (Figure 9) and should result in vibrational excitation of the products. This is corroborated by the NR spectra of **1H•**, which show substantial dissociation of $CH_3NH_2^{\bullet+}$ following collisional reionization of CH_3NH_2 (Figure 2).[33] Since the $\tilde{A}$ and $\tilde{B}$ states cross upon stretching the N−C bond to 1.75 Å, dissociation of **1H•** starting in the $\tilde{A}$ state can continue on the potential energy surface of the $\tilde{B}$ state and be funneled to the dissociative part of the ground state surface as discussed above. Hence, loss of methyl from both the $\tilde{A}$ and $\tilde{B}$ states is kinetically and dynamically possible. In contrast, N−H stretching faces large potential energy barriers in both $\tilde{A}$ and $\tilde{B}$ states, so that loss of H is prevented kinetically. It should be noted that the computational methods used in this study did not allow us to treat the ground and excited states at the same level of theory, and so the potential energy surfaces in the vicinity of the critical region of N−C bond cleavage could not be investigated in detail. Multireference calculations including perturbational treatment of electron correlation would be desirable to address these excited states comprehensibly and in more detail.[41,42]

The energy data allowed us to interpret some features of the neutralization−reionization and photoexcitation experiments. Regarding photoionization, the calculated energies suggested that the $(\tilde{D})^2A_1$ and higher states should be photoionizable by 2.41 and 2.54 eV photons, whereas the lower $(\tilde{A})^2B_1$ and $(\tilde{B})^2A_1$ states should not. The ionization energy of the $\tilde{C}$ state lies in between the photon energies. It should be noted that correlated calculations with large basis sets typically give ionization energies within 0.1 eV of accepted experimental values.[17,43] The 0.03−0.06 eV differences between the calculated ionization energies of the $(\tilde{B})^2A_1$ and $(\tilde{C})^2B_2$ states and the 488 nm photon

energy are well within this uncertainty range. However, even if the ionization energies of the $\tilde{B}$ and $\tilde{C}$ states had matched the photon energy, threshold photoionizations would have been expected to have very low cross sections.[15] The fact that metastable **1D•** and **2H•** were not photoionized at 2.41 and 2.54 eV excluded the $(\tilde{D})^2A_1$ and higher excited states and left the $\tilde{A}$, $\tilde{B}$, and $\tilde{C}$ states as the likely candidates for the observed metastability.

The role of excited states in **1H•** can be further discussed in view of the possible spontaneous or laser-induced de-excitation. The C_{2v} symmetry of **1H•** allows for all radiative transitions except for $A_1 \rightarrow A_2$ and $B_1 \rightleftarrows B_2$. Higher excited states therefore could be depopulated by spontaneous or stimulated photon emission in the laser beam, depending on the corresponding transition moments. The calculated oscillator strengths for the $\tilde{A} \rightarrow \tilde{X}$, $\tilde{B} \rightarrow \tilde{X}$, and $\tilde{C} \rightarrow \tilde{X}$ transitions, 0.23, 0.10, and 0.20, respectively, indicated excited-state lifetimes of $\tau < 0.46$ μs, according to eq 12, where m_e is the mass of electron, e is the elementary charge, ϵ_0 is the permeability of vacuum, c is the speed of light, $\tilde{\nu}_{ij}$ is the transition wavenumber, and f_{ij} is the oscillator strength.[44]

$$\tau = \frac{\epsilon_0 m_e c}{e^2 \pi \tilde{\nu}_{ij}^2 f_{ij}} \qquad (12)$$

Hence the calculated lifetimes would allow for <0.1% of metastable **1H•** surviving for 3.3 μs on the experimental time scale. It should be noted that oscillator strengths are difficult to calculate accurately even for simple systems, and substantially different values were obtained for ammonium radicals that depended on the computational method used.[14d,h] However, the oscillator strengths calculated for **1H•** were found to depend on the molecular geometry and decreased markedly upon stretching the N−H and N−C bonds (Table 2). In particular, the $\tilde{B} \rightarrow \tilde{X}$ transitions showed $f_{ij} \approx 0.06$ at d(N−H) = 1.25 Å or d(N−C) = 1.75 Å (Table 2), which pointed to $\tau \approx 0.92$ μs and 3% of metastable **1H•** surviving for 3.3 μs. The oscillator strengths for the $\tilde{A} \rightarrow \tilde{X}$ and $\tilde{C} \rightarrow \tilde{X}$ transitions decreased to 0.06 and 0.1, respectively, at d(N−H) = 1.35 Å, but remained high at larger N−C separations. This dependence may give a clue to the observed increase of the metastable **1H•** fractions with the precursor ion internal energy (vide supra). **1H•** formed by collisional electron transfer in a vibrationally excited $\tilde{B}$ state can be expected to have a low probability for radiative transition to the dissociative ground state.

The dramatic effect on metastability of deuterium isotope substitution in **1H•** is difficult to explain in the absence of detailed information on the properties of the excited states. It may be noted, however, that **1H•** and **2D•**, which were not metastable, showed strong coupling between the N−H and C−H or N−D and C−D stretching vibrational modes, respectively, whereas the N−D and C−H modes in **1HD•** and **1D•** and the N−H and C−D modes in **2H•** were well separated. If vibronic coupling plays a role in transitions through conical intersection to the dissociative $(\tilde{X})^2A_1$ state, the separation of the N−H and N−D modes may contribute to the observed metastability.

Conclusions

Isotopomers of dimethylammonium radicals showed metastability on the microsecond time scale when formed by collisional neutralization of dimethylammonium cations. Photolysis of the metastable radicals at 488 and 514.5 nm resulted in photoexcitation but not photoionization. The metastability of dimethylammonium radicals, the branching ratios in the N−H and N−C bond dissociations, and the isotope effects on loss of H or D could not be explained by the properties of the $(\tilde{X})^2A_1$ electronic ground state alone. Formation of metastable excited states is therefore suggested on the basis of experimental data and limited ab initio calculations. The $(\tilde{B})^2A_1$ state is predicted to have radiative lifetimes compatible with the observed metastability and can undergo methyl loss by nonradiative transition to the dissociative part of the ground state potential energy surface. A detailed theoretical investigation of the potential energy surfaces in the excited states of dimethylammonium appears to be necessary to explain the subtleties of this radical species' unusual behavior.

Acknowledgment. Support of this work by the National Science Foundation (Grant CHE-9412774) is gratefully acknowledged. The ab initio computations were conducted by using the resources of the Cornell Theory Center, which receives major funding from the National Science Foundation and New York State with additional support from the Advanced Research Projects Agency, the National Center for Research Resources at the National Institutes of Health, IBM Corporation, and members of the Corporate Research Institute. We also thank Dr. A. I. Boldyrev for providing us with vibrational frequencies of the transitions states.

References and Notes

(1) Herzberg, G. *Discuss. Faraday Soc.* **1981**, *71*, 165.

(2) Schuller, H.; Michel, A.; Grun, A. E. *Z. Naturforsch.* **1955**, *10A*, 1.

(3) (a) Alberti, F.; Huber, K. P.; Watson, J. K. G. *J. Mol. Spectrosc.* **1984**, *107*, 133. (b) Watson, J. K. G.; Majewski, W. A. *J. Mol. Spectrosc.* **1986**, *115*, 82.

(4) (a) Williams, B. W.; Porter, R. F. *J. Chem. Phys.* **1980**, *73*, 5598. (b) Gellene, G. I.; Cleary, D. A.; Porter, R. F. *J. Chem. Phys.* **1982**, *77*, 3471. (c) Jeon, S.-J.; Raksit, A. B.; Gellene, G. I.; Porter, R. F. *J. Am. Chem. Soc.* **1985**, *107*, 4129. (d) Griffiths, W. J.; Harris, F. M.; Beynon, J. H. *Int. J. Mass Spectrom. Ion Processes* **1987**, *77*, 233.

(5) (a) Gellene, G. I.; Porter, R. F. *J. Chem. Phys.* **1984**, *81*, 5570. (b) Raksit, A. B.; Jeon, S.-J.; Porter, R. F. *J. Phys. Chem.* **1986**, *90*, 2298. (c) Raksit, A. B.; Porter, R. F. *J. Chem. Soc., Chem. Commun.* **1987**, 500. (d) Raksit, A. B.; Porter, R. F. *Org. Mass Spectrom.* **1987**, *22*, 410. (e) Holmes, J. L.; Sirois, M. *Org. Mass Spectrom.* **1990**, *25*, 481. (f) Sirois, M.; George, M.; Holmes, J. L. *Org. Mass Spectrom.* **1994**, *29*, 11. (g) Wesdemiotis, C.; Fura, A.; McLafferty, F. W. *J. Am. Soc. Mass Spectrom.* **1991**, *2*, 459.

(6) Sadílek, M.; Tureček, F. *J. Phys. Chem.* **1996**, *100*, 9610, 15027.

(7) (a) Lewis, G. N. *J. Am. Chem. Soc.* **1916**, *38*, 762. (b) Reed, A. E.; Schleyer, P. v. R. *J. Am. Chem. Soc.* **1990**, *112*, 1434.

(8) Holmes, J. L. *Mass Spectrom. Rev.* **1989**, *8*, 513.

(9) Shaffer, S. A.; Tureček, F. *J. Am. Chem. Soc.* **1994**, *116*, 8647.

(10) Frøsig, L.; Wolken, J. K.; Tureček, F.; Nguyen, V. Q. *Proceedings of the 44th ASMS Conference on Mass Spectrometry and Allied Topics*, Portland, OR, May 1996; American Society for Mass Spectrometry, p 95.

(11) (a) Shaffer, S. A.; Sadílek, M.; Tureček, F. *J. Org. Chem.* **1996**, *61*, 5234. (b) Beranova, S.; Wesdemiotis, C. *Int. J. Mass Spectrom. Ion Processes* **1994**, *134*, 83.

(12) Shaffer, S. A.; Tureček, F. *J. Am. Soc. Mass Spectrom.* **1995**, *6*, 1004.

(13) Demolliens, A.; Eisenstein, O.; Hiberty, P. C.; Lefour, J. M.; Ohanessian, G.; Shaik, S. S.; Volatron, F. *J. Am. Chem. Soc.* **1989**, *111*, 5623.

(14) (a) Raynor, S.; Hershbach, D. R. *J. Phys. Chem.* **1982**, *86*, 3592. (b) Havriliak, S.; King, H. F. *J. Am. Chem. Soc.* **1983**, *105*, 4. (c) Cardy, H.; Kiotard, D.; Dargelos, A.; Poquet, E. *Chem. Phys.* **1983**, *77*, 287. (d) Havriliak, S.; Furlani, T. R.; King, H. F. *Can. J. Phys.* **1984**, *62*, 1336. (e) Kaspar, J.; Smith, V. H., Jr.; McMaster, B. N. *Chem. Phys.* **1985**, *96*, 81. (f) Kassab, E.; Evleth, E. *J. Am. Chem. Soc.* **1987**, *109*, 1653. (g) Wang, J.; Boyd, R. J. *Can. J. Phys.* **1994**, *72*, 851. (h) Martin, I.; Lavin, A. C.; Velasco, M.; Martin, M. O.; Karwowski, J.; Diercksen, G. H. F. *Chem. Phys.* **1996**, *202*, 307.

(15) Fuke, K.; Takasu, R.; Misaizu, F. *Chem. Phys. Lett.* **1994**, *229*, 597.

(16) Sadílek, M.; Tureček, F. *Chem. Phys. Lett.* **1996**, *263*, 203.

(17) Boldyrev, A. I.; Simons, J. *J. Chem. Phys.* **1992**, *97*, 6621.

(18) Lias, S. G.; Bartmess J. F.; Liebman, J. E.; Holmes, J. L.; Levin, R. D.; Mallard, G. W. *J. Phys. Chem. Ref. Data* **1988**, *17*, Suppl. 1.

(19) Lorquet, J.-C.; Leyh-Nihant, B.; McLafferty, F. W. *Int. J. Mass Spectrom. Ion Processes* **1990**, *100*, 465.

(20) Foresman, J. B.; Head-Gordon, M.; Pople, J. A.; Frisch, M. J. *J. Phys. Chem.* **1992**, *96*, 135.
(21) (a) Robinson, P. J.; Holbrook, K. A. *Unimolecular Reactions*; Wiley-Interscience: New York, 1972. (b) Gilbert, R. G.; Smith, S. C. *Theory of Unimolecular and Recombination Reactions*; Blackwell: London, 1990.
(22) Tureček, F.; Gu, M.; Shaffer, S. A. *J. Am. Soc. Mass Spectrom.* **1992**, *3*, 493.
(23) (a) Kuhns, D. W.; Tran, T. B.; Shaffer, S. A.; Tureček, F. *J. Phys. Chem.* **1994**, *98*, 4845. (b) Kuhns, D. W.; Tureček, F. *Org. Mass Spectrom.* **1994**, *29*, 463.
(24) (a) Sadílek, M.; Tureček, F. *J. Phys. Chem.* **1996**, *100*, 9610.
(25) (a) Hepburn, J. W. *Chem. Soc. Rev.* **1996**, 281. (b) Gellene, G. I.; Porter, R. F. *Acc. Chem. Res.* **1990**, *23*, 141.
(26) Frisch, M. J.; Trucks, G. W.; Head-Gordon, M.; Gill, P. M. W.; Wong, M. W.; Foresman, J. B.; Johnson, B. G.; Schelegel, H. B.; Robb, M. A.; Replogle, E. S.; Gomperts, R.; Andres, J. L.; Raghavachari, K.; Binkley, J. S.; Gonzalez, C.; Martin, R. L.; Fox, D. J.; DeFrees, D. J.; Baker, J.; Stewart, J. J. P.; Pople, J. A. *Gaussian 92*, Revision C; Gaussian Inc.: Pittsburgh, PA, 1992.
(27) Schlegel, H. B. *J. Chem. Phys.* **1986**, *84*, 4530.
(28) (a) Nobes, R. H.; Rodwell, W. R.; Bouma, W. J.; Radom, L. *J. Am. Chem. Soc.* **1981**, *103*, 1913. (b) McKee, M. L.; Lipscomb, W. N. *J. Am. Chem. Soc.* **1981**, *103*, 4673.
(29) Zhu, L.; Hase, W. L. *Quantum Chemistry Program Exchange*; Indiana University: Bloomington, IN, 1994; Program No. QCPE 644.
(30) Whitten, G. Z.; Rabinovitch, B. S. *J. Chem. Phys.* **1963**, *38*, 2466.
(31) Zhu, L.; Hase, W. L. *Chem. Phys. Lett.* **1990**, *175*, 117.
(32) From revised proton affinities, see: Szulejko, J. A.; McMahon, T. B. *J. Am. Chem. Soc.* **1993**, *115*, 7839.
(33) Nguyen, V. Q.; Tureček, F. *J. Mass Spectrom.* **1996**, *31*, 843.
(34) Note that residual $\mathbf{1HD}^+$, which shows at *m/z* 47 in the spectrum of $\mathbf{1D}^+$ (Figure 3a, inset), cannot cause serious contamination of the surviving $\mathbf{1D}^+$ ion, because the $\mathbf{1HD}^+$ ^{13}C and ^{15}N isotopomers also form hypervalent radicals upon neutralization.
(35) Derrick, P. J. *Mass Spectrom. Rev.* **1983**, *2*, 285.
(36) *UV Atlas of Organic Compounds*; Butterworths: London, 1966.
(37) Kimura, K.; Katsumata, S.; Achiba, Y.; Yamazaki, T.; Iwata, S. *Handbook of He(I) Photoelectron Spectra of Fundamental Organic Molecules*; Japan Scientific Press: Tokyo, 1981; pp 114, 120.
(38) Lowe, J. P. *Quantum Chemistry*, 2nd ed.; Academic Press: New York, 1993; p 96.
(39) Boesl, U.; Grotemeyer, J.; Muller-Dethlefs, K.; Neusser, H. J.; Selzle, H. L.; Schlag, E. W. *Int. J. Mass Spectrom. Ion Processes* **1992**, *118/119*, 191.
(40) Chupka, W. A. *J. Chem. Phys.* **1993**, *99*, 5800.
(41) Bernardi, F.; Olivucci, M.; Robb, M. A. *Pure Appl. Chem.* **1995**, *67*, 17.
(42) Roos, B. O. *Adv. Chem. Phys.* **1987**, *69*, 399.
(43) Turecek, F.; Cramer, C. J. *J. Am. Chem. Soc.* **1995**, *117*, 12243.
(44) Hollas, J. M. *Modern Spectroscopy*, 3rd ed.; Wiley: Chichester, 1996; pp 27−31.